

Combining weak and strong lensing in cluster potential reconstruction

Marcello Cacciato¹, Matthias Bartelmann², Massimo Meneghetti², Lauro Moscardini¹

¹ Dipartimento di Astronomia, Università di Bologna, via Ranzani 1, I-40127 Bologna, Italy

² Zentrum für Astronomie, ITA, Universität Heidelberg, Albert-Überle-Str. 2, D-69120 Heidelberg, Germany

Astronomy & Astrophysics, submitted

Abstract. We propose a method for recovering the two-dimensional gravitational potential of galaxy clusters which combines data from weak and strong gravitational lensing. A first estimate of the potential from weak lensing is improved at the approximate locations of critical curves. The method is fully linear and does not rely on the existence and identification of multiple images. We use simulations to show that it recovers the surface-mass density profiles and distributions very accurately.

1. Introduction

Weak gravitational lensing constrains the projected mass distributions of galaxy clusters with an angular resolution of $\gtrsim 0.5'$, while strong lensing occurs typically not farther than $(0.5-1)'$ from cluster cores. Nonetheless, both phenomena are due to the same gravitational potential. Recent observations of galaxy clusters with the ACS camera on-board HST have revealed large numbers of arcs in individual galaxy clusters, for which Abell 1689 is an outstanding example. In such clusters, strongly lensed images provide numerous constraints on the lensing potential, and the question is raised how weak and strong lensing are best combined in joint reconstructions of the lensing mass distribution.

Several methods were recently proposed which rely on the identification of multiply-imaged systems (Bradač et al. 2005a,b; Diego et al. 2005). We propose an alternative method here for which multiple images are not necessary and do not need to be identified. Based on a least- χ^2 minimisation, a first estimate of the lensing potential is obtained from weak-lensing alone, following the approach suggested by Bartelmann et al. (1996) and Seitz et al. (1998). Where the position of critical curves can be approximately identified due to the presence of strongly-lensed images, this estimate is improved by requiring that the determinant of the Jacobian matrix vanish. The method is easily generalised to sources at different redshifts. It is fully linear and allows deviations from the strict weak-lensing limit to be accounted for by a simple iterative algorithm.

After reviewing the necessary formalism of gravitational lensing in Sect. 2, we describe the method in Sect. 3 and illustrate it with simulations in Sect. 4. Conclusions are given in Sect. 5, and technical detail is summarised in the Appendix.

2. Basic formalism

We start by reviewing the basic formalism for gravitational lensing as we shall need it in the course of the paper. Since we are dealing with isolated lensing systems such as galaxy clusters, we can adopt the thin-lens approximation, according to which the lensing mass distribution is projected onto a lens plane perpendicular to the line-of-sight. Sources are located on source planes which are also perpendicular to the line-of-sight. The lens system is characterised by the three angular-diameter distances $D_{l,s,ls}$ between the observer and the lens, the source, and between lens and source, respectively.

All relevant properties of the lens system are then contained in the scalar lensing potential ψ , which is the suitably projected and rescaled Newtonian gravitational potential Φ of the lens,

$$\psi(\theta) = \frac{2}{c^2} \frac{D_{ls}}{D_l D_s} \int \Phi(D_l \theta) dz \quad (1)$$

(e.g. Schneider et al. 1992). Obviously, the lensing potential depends on the source redshift. Assuming that the lensing mass distribution is the same for sources on different source planes, we can still introduce a single scalar potential $\bar{\psi}(\theta)$ for a fiducial source redshift \bar{z}_s , and then scale the potential to other source redshifts z_s according to

$$\psi(\theta, z_s) = \bar{\psi}(\theta) \frac{D_{ls}(z_s)}{D_s(z_s)} \frac{D_s(\bar{z}_s)}{D_{ls}(\bar{z}_s)} . \quad (2)$$

The linearity of this transformation allows the reconstruction of the single, fiducial lensing potential $\bar{\psi}$ from sources on multiple source planes.

The two-dimensional, projected mass distribution of the lens is described by the convergence κ , while the distortions caused by the lens are characterised by the trace-free, symmet-

ric shear tensor with the two components $\gamma_{1,2}$. Both are linear combinations of second derivatives of ψ ,

$$\gamma_1 = \frac{1}{2} (\psi_{,11} - \psi_{,22}) , \quad \gamma_2 = \psi_{,12} , \quad \kappa = \frac{1}{2} \nabla^2 \psi . \quad (3)$$

The convergence is the surface mass density Σ in units of its critical value

$$\Sigma_{\text{cr}} = \left(\frac{4\pi G}{c^2} \frac{D_l D_{\text{ls}}}{D_s} \right)^{-1} . \quad (4)$$

The lens mapping relates the source position β to the image position(s) θ ,

$$\beta = \theta - \nabla \psi(\theta) . \quad (5)$$

For sources which are small compared to typical scales of the (reduced) deflection angle $\alpha = \nabla \psi$, the lens mapping can be linearised. Imaging is then locally characterised by the Jacobian matrix

$$\mathcal{A} = \frac{\partial \beta}{\partial \theta} = \begin{pmatrix} 1 - \kappa - \gamma_1 & -\gamma_2 \\ -\gamma_2 & 1 - \kappa + \gamma_1 \end{pmatrix} . \quad (6)$$

This shows that κ is responsible for isotropically shrinking or stretching images, while γ causes anisotropic deformation.

A sufficiently small circular source of radius r is imaged as an ellipse with semi-major and -minor axes $a = r(1 - \kappa - \gamma)^{-1}$ and $b = r(1 - \kappa + \gamma)^{-1}$, respectively. The ellipticity, defined as $\varepsilon \equiv (a - b)/(a + b)$, is thus

$$\varepsilon = \frac{\gamma}{1 - \kappa} \equiv g , \quad (7)$$

defining the so-called *reduced shear* g . In the weak-lensing regime, characterised by $\kappa \ll 1$ and $\gamma_{1,2} \ll 1$, the ellipticity approximates the shear, $\varepsilon \approx \gamma$. In gravitational lenses capable of strong lensing, the weak-lensing approximation typically fails very close to the centre. While the linear relation between ellipticity and shear can then be applied in the outskirts of the lens, corrections may become necessary near the core.

Critical curves θ_c are closed curves in the lens plane consisting of points where \mathcal{A} cannot be inverted, $\det \mathcal{A}(\theta_c) = 0$. Their images in the source plane under the lens mapping (5) are called caustics; they are given by $\beta_c = \theta_c - \nabla \psi(\theta_c)$. Obviously, the relation

$$(1 - \kappa)^2 - \gamma^2 = 0 \quad (8)$$

is satisfied along critical curves.

Any measurement of gravitational lensing which is based on local distortion information alone cannot distinguish between lensing with the Jacobian matrices \mathcal{A} and $\lambda \mathcal{A}$, with $\lambda \neq 0$. The matrix $\lambda \mathcal{A}$ produces images which are isotropically stretched by the factor λ , but with identical ellipticity ε as the matrix \mathcal{A} . This invariance against the transformation $\mathcal{A} \rightarrow \lambda \mathcal{A}$ causes κ and γ to be invariant against the transformation

$$\kappa \rightarrow (1 - \lambda) + \lambda \kappa , \quad \gamma \rightarrow \lambda \gamma , \quad (9)$$

which obviously leaves the reduced shear (7) invariant. This invariance transformation was first described as a “mass-sheet

degeneracy” (Falco et al. 1985; Schneider & Seitz 1995) because it tends to $\kappa \rightarrow (1 - \lambda) + \kappa$ in the limit of $|1 - \lambda| \rightarrow 0$.

We emphasise in the context of our joint reconstruction method that the critical curves are also invariant under the transformation (9). Obviously, the defining condition $\det \mathcal{A} = 0$ for critical curves is unchanged if \mathcal{A} is multiplied by $\lambda \neq 0$. Translated to the underlying lensing potential, the transformation (9) allows transformations of the potential of the form

$$\psi \rightarrow \lambda \psi + \frac{1 - \lambda}{4} (\theta_1^2 + \theta_2^2) + a\theta_1 + b\theta_2 + c , \quad (10)$$

with arbitrary constants a , b and c . We shall later make use of this transformation for adjusting the lensing potential obtained from weak- and strong-lensing constraints.

3. Outline of the method

3.1. Weak lensing

We propose to combine local constraints from weak and strong lensing on the lensing potential ψ in the reconstruction of two-dimensional lensing mass distributions. We aim at the lensing potential because it is the smoothest lensing quantity available and because it provides a complete description of all lensing phenomena at least in the approximation of a single-lens plane. The lens is covered by a grid, the values ψ_i of the lensing potential in the grid cells are considered as the model parameters, and the method seeks to find a set of potential values $\{\psi_i\}$ such that the agreement between the data and the model is optimised in a least- χ^2 sense.

Our χ^2 function is a sum of two terms, χ_w^2 and χ_s^2 , encoding the information provided by weak and strong lensing, respectively. An obvious choice for the contribution of weak-lensing information to χ^2 is

$$\chi_w^2 = \sum_{i=1}^n \frac{|\varepsilon_i - \gamma_i(\psi_j)|^2}{\sigma_{wi}^2} , \quad (11)$$

where n is the number of cells in the grid covering the lens plane. In each cell, the mean measured ellipticity of lensed source galaxies, ε_i , is compared to its expectation value, which is γ_i in the weak-lensing regime.

If the weak-lensing approximation is not valid, γ_i must be replaced by the reduced shear $g_i \equiv \gamma_i/(1 - \kappa_i)$ in (11). This leads to a non-linear dependence between measured ellipticities and the deflection potential, which is most conveniently addressed in an iterative procedure. Starting from $\kappa_i^{(0)} = 0$ on all grid cells, subsequent iterative approximations $\{\psi_i^{(k)}\}$ to the lensing potential are found by minimising

$$\chi_w^2 = \sum_{i=1}^n \frac{1}{\sigma_{wi}^2} \left| \varepsilon_i - \frac{\gamma_i(\psi_j^{(k+1)})}{1 - \kappa_i^{(k)}} \right|^2 . \quad (12)$$

The grid resolution must be chosen such that grid cells are large enough for reasonably accurate measurements of source ellipticities, and yet small enough that the lensing potential ψ does not change appreciably across a grid cell. We adopt the

common assumption that intrinsic source ellipticities are randomly oriented and thus tend to zero when averaged within sufficiently large samples. The typical standard deviation of intrinsic ellipticities from zero is $\sigma_\epsilon \approx 0.3$ (Brainerd et al. 1996). Requiring that the noise of a shear measurement within a grid cell due to the intrinsic ellipticities be at or below the level of 10%, we need to average over a number N of galaxies determined by

$$\frac{\sigma_\epsilon}{\sqrt{N}} \approx \frac{0.3}{\sqrt{N}} \lesssim 0.1, \quad (13)$$

thus $N \gtrsim 10$. At a surface density of, say, 30 arcmin^{-2} for the background sources, this implies grid cells of $\gtrsim 35''$ side length. In the “concordance” Λ CDM cosmology, $1h^{-1}\text{Mpc}$ spans $\sim 5'$ at redshift ~ 0.3 . The virial diameter of a massive cluster at that redshift is thus contained in fields of $\sim (10' \times 10')$, approximately corresponding to $\sim (20 \times 20)$ pixels. This illustrates the grid resolution which we can expect weak-lensing cluster mass reconstructions to achieve. Then, the typical noise level σ_{wi} per pixel is ≈ 0.1 , as follows from (13).

So far, we have essentially reviewed the cluster reconstruction approach proposed by Bartelmann et al. (1996) and extended by maximum-entropy regularisation in Seitz et al. (1998). While it was suggested in Bartelmann et al. (1996) to minimise χ_w^2 with the conjugate-gradient method, the finite differencing of the gridded lensing potential needed to obtain expectations for γ_i implies that, in the weak-lensing regime,

$$\frac{\partial \chi_w^2}{\partial \psi_i} = 0 \quad (14)$$

is a linear equation in the ψ_i which can be solved using matrix inversion. This was noted by Bradač et al. (2005a,b), who have recently proposed and applied another algorithm for combining weak and strong cluster lensing. If the weak-lensing approximation does not hold, this linear relation is formally destroyed, but the iterative procedure outlined in (12) restores it. The ψ_i are thus obtained from

$$\psi_j = \mathcal{B}_{jk}^{-1} \mathcal{V}_k, \quad (15)$$

with a sparse matrix \mathcal{B} and a data vector \mathcal{V} .

The main difference between the algorithms proposed by Bradač et al. (2005b) and here is the way how constraints from strong lensing are taken into account. While the method by Bradač et al. (2005b) uses information from multiply-imaged sources, we advocate constraining the potential using the (approximate) knowledge of the critical curves from the location of large arcs.

Another cluster reconstruction procedure was recently proposed by Diego et al. (2005) which also combines weak and strong-lensing data. Their idea is to expand the projected cluster mass distribution into a set of basis functions which are then constrained individually using shear and strong-lensing data. The minimisation then proceeds iteratively, using an adaptive grid to cover the cluster field.

3.2. Strong lensing

Strong lensing in clusters gives rise to highly distorted large arcs which occur in the immediate vicinity of critical curves in the lens plane. There, by definition (8), the positions of large arcs approximate the locations where $\det \mathcal{A} = 0$. If written in terms of the lensing potential ψ , this condition translates into an expression which is quadratic in the second derivatives of ψ .

We suppose that a solution ψ_j has already been obtained from weak lensing using (15). It exists on a coarse grid adapted to the low resolution of weak-lensing measurements. This grid is now refined near the cluster core to a resolution adapted to the critical curve(s). Since strong lensing typically occurs within the innermost arc minute around the cluster core, this grid will be much finer and smaller than the grid introduced for weak lensing. It can thus be introduced as a sub-grid which improves the resolution of the few central cells of the weak-lensing grid which contain the large arcs, and thus parts of the critical curve.

In the idealised case of a known critical curve, we could identify a continuous chain of sub-grid cells following the critical curve. Let the number of these cells be n^* , then the contribution of strong lensing to the χ^2 function could be

$$\chi_s^2 = \sum_{i=1}^{n^*} \frac{(\det \mathcal{A})_i^2}{\sigma_{si}^2} = \sum_{i=1}^{n^*} \frac{[(1 - \kappa)^2 + |\gamma|^2]^2}{\sigma_{si}^2}, \quad (16)$$

expressing the expectation that the Jacobian determinant be zero within the tolerance expressed by σ_{si} in all sub-grid pixels covering the critical curve.

The sub-grid resolution has to be high enough to follow the critical curve with sufficient accuracy. The tolerance σ_{si} quantifies tolerable deviations of $(\det \mathcal{A})_i$ from zero. It combines the uncertainty in the position of the critical curve, which must be estimated from the observed arc positions, and the deviation of $\det \mathcal{A}$ from zero expected within one sub-grid pixel.

The second contribution can be suppressed to a negligible level because we are free to choose the sub-grid resolution. The first contribution can be estimated as follows: since $\det \mathcal{A} = 0$ on the critical curve, its deviation from zero at a distance $\delta\theta$ is

$$\sigma_s \approx \left. \frac{\partial \det \mathcal{A}}{\partial \theta} \right|_{\theta_c} \delta\theta \approx \frac{\delta\theta}{\theta_E}, \quad (17)$$

approximating the derivative of the Jacobian determinant at the critical curve by the inverse of the Einstein angle θ_E . This is exact for the tangential arcs formed by an isothermal sphere, and reasonably accurate for similar lens models. Assuming uncertainties in the positions of critical curves of order $\delta\theta \approx 1''$ and Einstein radii of order $\approx 30''$, we find $\sigma_s \approx 3 \times 10^{-2}$.

We believe that this approach has two distinct advantages compared to methods using multiple images for constraining the lens model with strong-lensing data. First, it can be used simply based on the approximate knowledge of the location of the critical curves without the need to have or identify multiple arcs which are due to the same source. Prominent counter-arcs are often missing in strongly lensing clusters, which reflects their lack of axial symmetry (Grossman & Narayan 1988,

1989; Kovner 1989). Thus, methods relying on the identification of multiple images are only applicable to clusters which produce multiple large arcs, and in which the multiple images can be attributed to single sources with a high degree of certainty. Second, methods based on multiple images require that all images identified as belonging to the same source be imaged on a single source. Even if an assumed model satisfies this requirement, it must be tested whether the source would have any additional images which are not observed. However, the inversion of lens models which is necessary to search for all images of a source is a highly nonlinear procedure. It thus appears to us that the combination of weak and strong-lensing information by identifying critical curves (or parts thereof) has substantial advantages compared to methods identifying multiple images.

Arches in clusters may appear at different redshifts and thus trace different critical curves. Such information can be built into the χ^2 function by means of the redshift scaling (2). This could be achieved by identifying one critical curve (or arc system) as fiducial with a redshift \bar{z}_s , and to scale the critical curves for all other systems according to their (spectroscopic or photometric) redshift by applying appropriate distance factors to the lensing potential ψ .

3.3. χ^2 minimisation

The weak-lensing solution ψ_i obtained on the coarse grid is improved on the fine grid in the following way. Bi-cubic interpolation is used on the reconstructed potential near the cluster core in order to reach a resolution which is high enough to incorporate the constraints from strong lensing. We emphasise that the interpolation is carried out on the lensing potential because it is the smoothest quantity at hand, and that the interpolation scheme has to be of sufficiently high order for the convergence and the shear to be continuous. In fact, since second derivatives of the potential are needed, interpolation schemes up to second order will fail.

The location and shape of the fine grid on which the potential is interpolated from the weak-lensing solution depends entirely on the strong-lensing constraints. There can be single or multiple arc systems which constrain the Jacobian determinant to zero at isolated locations near the cluster cores, or approximations to the entire critical curve may be available from strong-lensing reconstructions of parametrised cluster mass models. For simplicity, we perform the interpolation of the potential on a square-shaped grid enclosing all critical curves of our model cluster.

On the fine grid, the interpolated weak-lensing solution ψ_i^* is improved by requiring

$$\frac{\partial \chi_w^2}{\partial \psi_i^*} = -\frac{\partial \chi_s^2}{\partial \psi_i^*}, \quad (18)$$

which leads to the set of linear equations for ψ_k^* on the fine grid

$$\mathcal{B}_{jk} \psi_k^* = \mathcal{V}_j - \mathcal{T}_j, \quad (19)$$

where \mathcal{T}_j is a data vector containing the information on the critical curves. Details are shown in the Appendix. If the interpolated weak-lensing solution already satisfies $\det \mathcal{A} = 0$ along

the critical curve(s), $\mathcal{T}_j = 0$. Thus, \mathcal{T}_j quantifies by how much ψ_k^* needs to be corrected due to the strong-lensing constraints.

We point out again that the potential reconstructed from weak and strong lensing alike allows transformations of the form (10) because neither the weakly-lensed ellipticities nor the critical curves are changed by them. This allows smoothly matching the potential values on the fine and coarse grids.

4. Testing the method

4.1. Synthetic data

In order to test and illustrate the proposed method, we apply it to synthetic background images lensed by a simulated galaxy cluster taken from the set described in Bartelmann et al. (1998). The cluster was simulated within the ‘‘concordance’’ Λ CDM model with matter density $\Omega_{m0} = 0.3$, cosmological constant $\Omega_{\Lambda 0} = 0.7$ and Hubble parameter $h = 0.7$. Its redshift is $z = 0.35$, and its total mass is $1.4 \times 10^{15} M_\odot$. It is embedded in a cube of $5 h^{-1}$ Mpc (comoving) side length, corresponding to 17.8 arc minutes. At a coarse-grid resolution of 32×32 pixels, one pixel has a side length of $33''$, in good agreement with the resolution constraint estimated above.

Lensed data are synthesised by randomly distributing elliptical sources on the source plane, which we place at $z_s = 1$ for simplicity. The sources have random intrinsic orientations, axis ratios which are drawn randomly from the interval $[0.5, 1]$, and axes determined such that their area equals that of a circle with radius $0.5''$. Although this choice of source properties is simplified, it should be irrelevant for demonstrating the feasibility of our method.

Starting from the known lensing potential of the cluster (projected along the three axes of the simulation cube), weakly and strongly lensed images are produced from the synthetic background sources by tracing rays through the deflection-angle field, which is the gradient of the potential.

4.2. Results

Figure 1 shows the original and reconstructed radial convergence profiles. Far away from the cluster centre, the convergence is well recovered from weak-lensing data, but the central part suffers from the inevitable softening due to the resolution limit of weak lensing. This is corrected by adding the strong-lensing constraints. The agreement between the outer parts of the true profile and its weak-lensing reconstruction could be improved by means of the transformation (10), but this would not remove the central discrepancy.

Figure 2 shows two-dimensional reconstructions of two clusters after applying the strong-lensing correction at their cores. The coarse grid resolution far from the cluster centre is increased near the core where the critical curve of the cluster is located. The resolution of the fine grid is 16 times higher (per dimension) than that of the coarse grid, so that pixels of the fine grid have $\sim 2''$ side length.

The quality of the combined reconstruction is illustrated in Fig. 3 by a map of the relative differences between our reconstruction and the original convergence of the simulated clus-

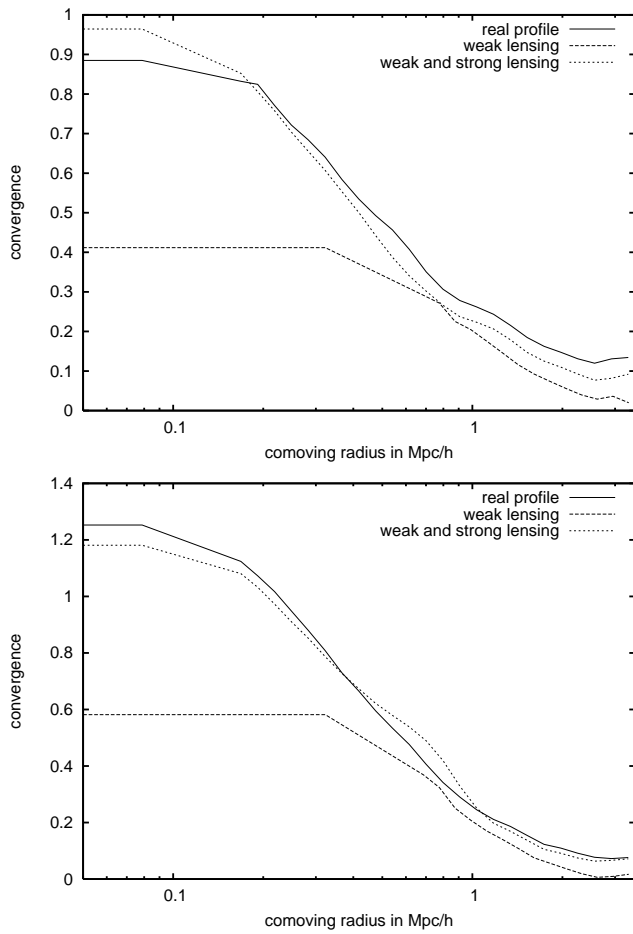


Fig. 1. Comparisons of the radial convergence profiles $\kappa(r)$ for two projections of the original cluster, their weak-lensing reconstructions, and the joint reconstructions after adding the strong-lensing constraints. While the profile obtained from weak lensing alone suffers from the inevitable softening, strong lensing considerably improves the agreement.

ter. Evidently, the mass distribution is well reproduced everywhere in the field (see the caption for a quantitative description), in agreement with the good recovery of the radial profile. Moreover, constraints from strong lensing substantially improve the reconstruction in the cluster core. This demonstrates that the algorithm is working as expected.

Figure 3 summarises the principal properties of our reconstruction method. The outer region (with low resolution) is well reproduced using only weak-lensing constraints, but the high-density peak near the cluster core is poorly resolved. The reconstruction of the core structure is greatly improved by adding the constraints from strong lensing. Given the quality of the results, we did not need to apply the iterative algorithm suggested above for correcting the relation between measured ellipticities and shear.

5. Conclusions

We have proposed a novel method for galaxy-cluster reconstruction which combines weak and strong-lensing data. The

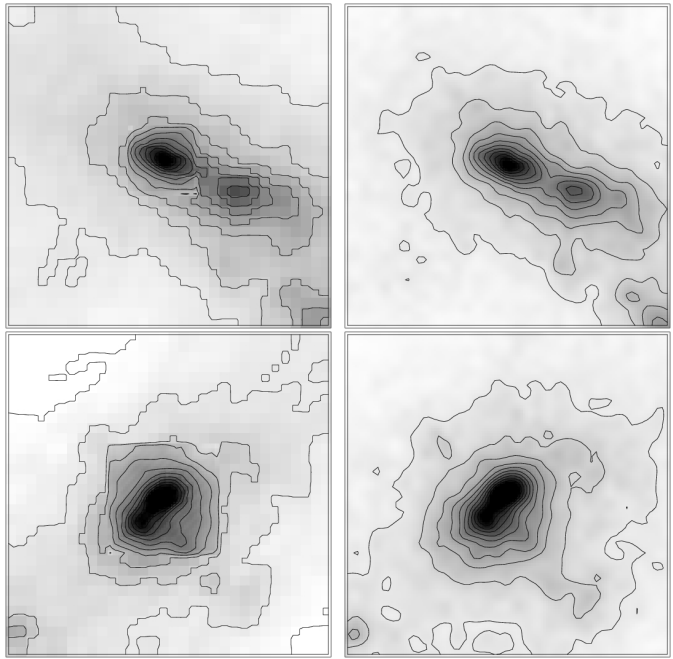


Fig. 2. Two simulated clusters are shown in the two rows. Their original convergence fields are displayed in the right column, their joint reconstructions using weak and strong lensing in the left. The colour scale is linear, the grey scales range from 0 to 1.1, and the contours are spaced by $\Delta\kappa = 0.1$.

method is based on a least- χ^2 fitting of the lensing potential ψ (Bartelmann et al. 1996; Seitz et al. 1998) and exploits the fact that the χ^2 minimisation can be carried out efficiently by inverting a sparse matrix (Bradač et al. 2005a,b). Contrary to other methods proposed for joining weak and strong lensing information (Bradač et al. 2005b; Diego et al. 2005), we propose to constrain the lensing potential obtained from the weak-lensing data by the approximate location of the critical curves, where the Jacobian determinant of the lens mapping must be close to zero.

The angular resolution which can be achieved by weak-lensing cluster reconstructions is typically of order $0.5'$ for background source densities near $(30 - 40) \text{ arcmin}^{-2}$. This is much too coarse for tracing critical curves, whose typical sizes are $(0.5 - 1)'$. Thus, we propose to cover those regions of the cluster fields with a refined grid where strong-lensing constraints are available.

We test the performance of the method on synthetic images produced with simulated lensing clusters. We conclude that the mass distribution in galaxy clusters is well reproduced across the entire field, in particular where constraints from strong lensing features are introduced. In practice, our algorithm first finds a lensing potential on the coarse grid which fits the weak-lensing data best. This approximation to the potential is then interpolated into the cells of the fine grid covering the critical curves or parts thereof, and refined by a χ^2 minimisation taking the strong-lensing constraints into account.

We have used several approximations here. First, we treat weak lensing to first order in the shear γ , i.e. we compare measured ellipticities to γ rather than the reduced shear $g =$

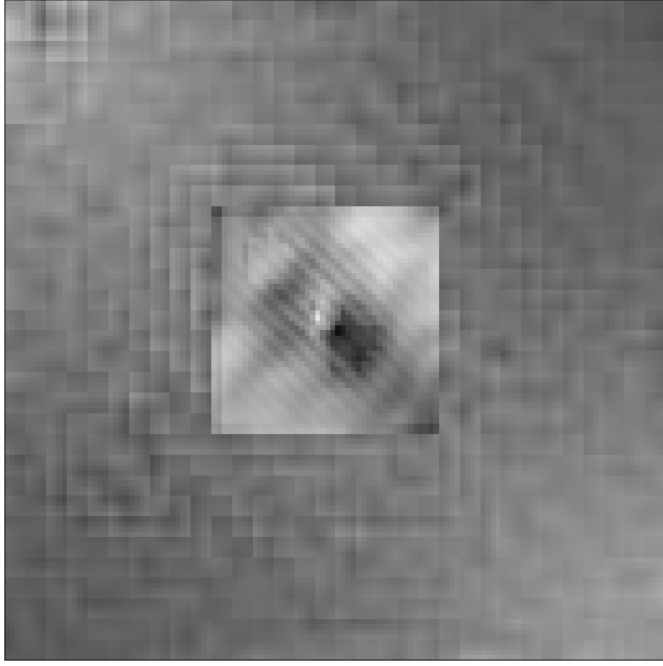


Fig. 3. Deviation of the reconstructed from the original convergence fields, κ and $\bar{\kappa}$, respectively. To avoid divergences near the field boundaries where both κ and $\bar{\kappa}$ are small, the grey scale encodes the relative difference between $(1 + \kappa)$ and $(1 + \bar{\kappa})$, i.e. $(\kappa - \bar{\kappa})/(2 + \kappa + \bar{\kappa})$. The grey scale ranges from -0.1 (white) to $+0.1$ (black). Obviously, the relative deviations are very small.

$\gamma(1 - \kappa)^{-1}$. Retaining the desirable linearity of the method, this can easily be overcome by introducing an iteration scheme in which the convergence κ reconstructed in the previous step is used to update the reduced shear of the current step (see also Bradač et al. 2005b). Given the quality of our simulated results, we did not need to use this iteration scheme.

Second, we have assumed knowledge of the entire critical curve, which is of course not directly observable. Cluster images such as those recently taken with ACS on-board HST, however, show so many large arcs that critical curves can in fact be well constrained all around the cluster cores. Furthermore, critical curves can reliably be inferred from parametrised strong-lensing models, in particular when combined with dynamical constraints from central cluster galaxies (e.g. Meneghetti et al. 2005).

Third, we have assumed the strongly-lensed sources to be all at the same redshift. If multiple arc systems at different redshifts are observed, a lensing potential can still be reconstructed for one fiducial source redshift \bar{z}_s by applying the distance correction factors defined in (2).

Thus, we believe that the simplifications used here are not at all restrictive, and that the method suggested here provides a useful alternative to those proposed earlier.

Acknowledgements. This work was supported by the Vigoni programme of the German Academic Exchange Service (DAAD) and Conference of Italian University Rectors (CRUI).

Appendix A: Linear equations for χ^2 minimisation

We summarise here some technical aspects of how the physical quantities κ and γ are related to the discretised deflection potential ψ in our approach.

Derivatives of ψ are replaced by common finite-differencing schemes. We use 9 grid points for κ , 7 grid points for γ_2 and 4 points for γ_1 . This allows any lensing quantity to be written as the multiplication of a well-defined matrix with the vector of lensing-potential values,

$$\kappa_i = \mathcal{K}_{ij} \psi_j \quad , \quad \gamma_i^1 = \mathcal{G}_{ij}^1 \psi_j \quad \text{and} \quad \gamma_i^2 = \mathcal{G}_{ij}^2 \psi_j . \quad (\text{A.1})$$

The matrices \mathcal{G}^i and \mathcal{K} are very sparse because the finite-differencing schemes use only near neighbours (cf. Bradač et al. 2005b). Algorithms exist for efficient inversion of such matrices.

Based on the finite-differencing schemes expressed by the matrix eqs. (A.1), the minimisation of χ^2 is reduced to a linear algebraic equation. Starting from the χ_w^2 for weak lensing, we have

$$\begin{aligned} 0 &= \frac{\partial \chi_w^2(\psi_k)}{\partial \psi_j} \\ &= -2 \sum_{i=1}^n \frac{1}{\sigma_{wi}^2} \left[(\varepsilon_i^1 - \gamma_i^1) \frac{\partial \gamma_i^1}{\partial \psi_j} + (\varepsilon_i^2 - \gamma_i^2) \frac{\partial \gamma_i^2}{\partial \psi_j} \right] \\ &= \sum_{i=1}^n \frac{-2}{\sigma_{wi}^2} \left[(\varepsilon_i^1 - \gamma_i^1) \frac{\partial (\mathcal{G}_{ik}^1 \psi_k)}{\partial \psi_j} + (\varepsilon_i^2 - \gamma_i^2) \frac{\partial (\mathcal{G}_{ik}^2 \psi_k)}{\partial \psi_j} \right] \\ &= \sum_{i=1}^n \frac{-2}{\sigma_{wi}^2} \left[(\varepsilon_i^1 - \gamma_i^1) \mathcal{G}_{ij}^1 \delta_{jk} + (\varepsilon_i^2 - \gamma_i^2) \mathcal{G}_{ij}^2 \delta_{jk} \right] \\ &= \sum_{i=1}^n \frac{-2}{\sigma_{wi}^2} \left[(\varepsilon_i^1 - \gamma_i^1) \mathcal{G}_{ij}^1 + (\varepsilon_i^2 - \gamma_i^2) \mathcal{G}_{ij}^2 \right] \\ &= \sum_{i=1}^n \frac{-2}{\sigma_{wi}^2} \left[\varepsilon_i^1 \mathcal{G}_{ij}^1 - \mathcal{G}_{ij}^1 \mathcal{G}_{ik}^1 \psi_k + \varepsilon_i^2 \mathcal{G}_{ij}^2 - \mathcal{G}_{ij}^2 \mathcal{G}_{ik}^2 \psi_k \right] \\ &= \sum_{i=1}^n \frac{2}{\sigma_{wi}^2} \left\{ \left[\mathcal{G}_{ji}^{1T} \mathcal{G}_{ik}^1 + \mathcal{G}_{ji}^{2T} \mathcal{G}_{ik}^2 \right] \psi_k - \left[\varepsilon_i^1 \mathcal{G}_{ij}^1 + \varepsilon_i^2 \mathcal{G}_{ij}^2 \right] \right\} , \quad (\text{A.2}) \end{aligned}$$

which can clearly be written in the form

$$\mathcal{B}_{jk} \psi_k = \mathcal{V}_j , \quad (\text{A.3})$$

with the matrix

$$\mathcal{B}_{jk} \equiv \sum_{i=1}^n \frac{1}{\sigma_{wi}^2} \left[\mathcal{G}_{ji}^{1T} \mathcal{G}_{ik}^1 + \mathcal{G}_{ji}^{2T} \mathcal{G}_{ik}^2 \right] \quad (\text{A.4})$$

and the data vector

$$\mathcal{V}_j = \sum_{i=1}^n \frac{1}{\sigma_{wi}^2} \left[\varepsilon_i^1 \mathcal{G}_{ij}^1 + \varepsilon_i^2 \mathcal{G}_{ij}^2 \right] . \quad (\text{A.5})$$

Similarly evaluating the constraints from strong lensing yields

$$\begin{aligned} \frac{\partial \chi_s^2}{\partial \psi_j^*} &= \frac{\partial}{\partial \psi_j^*} \left[\sum_{i=1}^{n*} \frac{(\det \mathcal{A}_i)^2}{\sigma_i^2} \right] \\ &= \sum_{i=1}^{n*} \frac{-4 \det \mathcal{A}_i}{\sigma_i^2} \left[(1 - \kappa_i) \frac{\partial \kappa_i}{\partial \psi_j^*} - \frac{\partial \gamma_i^1}{\partial \psi_j^*} - \frac{\partial \gamma_i^2}{\partial \psi_j^*} \right] \\ &= \sum_{i=1}^{n*} \frac{-4 \det \mathcal{A}_i}{\sigma_i^2} \left[(1 - \kappa_i) \mathcal{K}_{ij} - \gamma_i^1 \mathcal{G}_{ij}^1 - \gamma_i^2 \mathcal{G}_{ij}^2 \right] \\ &= \mathcal{T}_j , \quad (\text{A.6}) \end{aligned}$$

where the κ_i and the $\gamma_i^{1,2}$ are obtained from the interpolated weak-lensing solution.

On the refined grid, the χ^2 minimisation (A.3) is modified by

$$\mathcal{B}_{jk} \psi_k^* = \mathcal{V}_j - \mathcal{T}_j. \quad (\text{A.7})$$

Obviously, if the weak-lensing solution already satisfies $\det \mathcal{A} = 0$ on the critical curves, $\mathcal{T} = 0$ there, and no correction is necessary.

References

Bartelmann, M., Huss, A., Colberg, J. M., Jenkins, A., & Pearce, F. R. 1998, A&A, 330, 1

Bartelmann, M., Narayan, R., Seitz, S., & Schneider, P. 1996, ApJL, 464, L115

Bradač, M., Erben, T., Schneider, P., et al. 2005a, A&A, 437, 49

Bradač, M., Schneider, P., Lombardi, M., & Erben, T. 2005b, A&A, 437, 39

Brainerd, T. G., Blandford, R. D., & Smail, I. 1996, ApJ, 466, 623

Diego, J. M., Tegmark, M., Protopapas, P., & Sandvik, H. B. 2005, ArXiv Astrophysics e-prints, arXiv:astro-ph/0509103

Falco, E. E., Gorenstein, M. V., & Shapiro, I. I. 1985, ApJ, 289, L1

Grossman, S. A. & Narayan, R. 1988, ApJL, 324, L37

Grossman, S. A. & Narayan, R. 1989, ApJ, 344, 637

Kovner, I. 1989, ApJ, 337, 621

Meneghetti, M., Bartelmann, M., Jenkins, A., & Frenk, C. 2005, ArXiv Astrophysics e-prints; arXiv:astro-ph/0509323

Schneider, P., Ehlers, J., & Falco, E. E. 1992, Gravitational Lenses (Springer Verlag, Heidelberg)

Schneider, P. & Seitz, C. 1995, A&A, 294, 411

Seitz, S., Schneider, P., & Bartelmann, M. 1998, A&A, 337, 325